A $PbWO_4$-based Neutral Particle Spectrometer in Hall C at 12 GeV JLab

Tanja Horn

Catholic University of America, Washington, DC 20064, USA

E-mail: hornt@cua.edu

for the JLab Neutral Particle Spectrometer Collaboration

Abstract. The Neutral Particle Spectrometer is a standalone electromagnetic calorimeter capable of detecting high energy photons from, for instance, DVCS or π^0 decay with good energy and spatial resolution in a high rate environment. It can be used together with the Hall C high-momentum spectrometers for a suite of experiments with the underlying scientific objective of studying quark dynamics through exclusive and semi-inclusive reactions.

1. Introduction

Over the last decade, hard exclusive processes have emerged as a class of reactions providing novel information on the quark and gluon distributions in hadrons. This information is more complete than what can be obtained from studies of inclusive and elastic scattering alone [1, 2, 3]. QCD factorization theorems allow for expressing amplitudes of hard exclusive processes in terms of the Generalized Parton Distributions (GPDs) [4, 5], which are expected to provide a universal (process-independent) description of the nucleon, and have a known QCD (Q^2) evolution. GPDs are hybrid distributions that combine aspects of the usual collinear Parton Distribution Functions and elastic form factors. As such, GPDs simultaneously encode information on parton distributions and correlations in both momentum (in the longitudinal direction) and coordinate (in the transverse direction) spaces. An interesting aspect of GPDs is also their connection to the form factors of the energy-momentum tensor, which, among other things, establishes the decomposition of the proton spin in terms of the quark and gluon contributions to the total orbital momentum [6]. GPDs provide an unprecedented means to describe nucleon structure. The GPD program thus lies at the heart of the scientific motivation of 12 GeV JLab.

The Hall C 12 GeV base experimental equipment consists of two magnetic spectrometers: the High Momentum Spectrometer (HMS) and the Super High Momentum Spectrometer (SHMS). Important features of these magnetic spectrometers include their ability rotate around a pivot on a rigid support structure and a well-shielding detector enclosure. The acceptance of magnetic spectrometers is limited, but within this acceptance they provide excellent control over systematic uncertainties allowing for high precision cross section measurements [1]. Depending on the specific requirements of the experiments, the HMS and SHMS can detect either negatively

[1] This has been demonstrated by more than 200 Rosenbluth separations (close to 1000 kinematics).

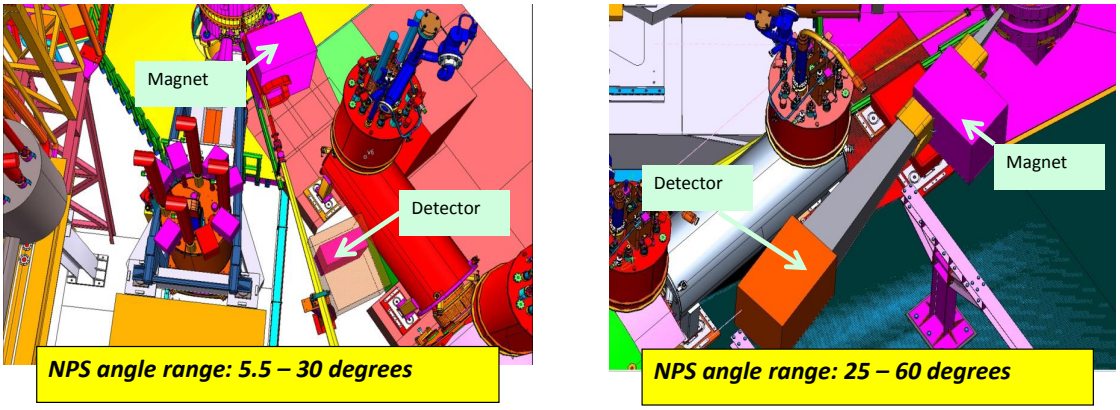

Figure 1. The Neutral Particle Spectrometer in Hall C at JLab.

or positively charged particles by choosing the magnetic field and the trigger configuration. However, additional instrumentation is needed to carry out the Hall C scientific program with neutral particle final states. The program consists of Exclusive Deeply Virtual Compton and π^0 precision cross section measurements, measurements of the SIDIS π^0 production as validation of factorization, and Wide-Angle Compton Scattering and exclusive photoproduction of π^0 mesons at large angles.

The Neutral Particle Spectrometer (NPS) is envisioned as a facility utilizing the well-understood HMS and the infrastructure of the SHMS to allow for precision (coincidence) cross section measurements of neutral particles. It can be cantelevered off the SHMS platform covering spectrometer angles between 5.5 and 30 degrees and be installed on the SHMS platform to cover angles between 25 and 60 degrees as illustrated in Fig. 1.

2. Physics with neutral final states

The best studied hard exclusive process is Deeply Virtual Compton Scattering (DVCS). Present analyses assume validity of twist-2 dominance, and a leading order formalism. The GPD program at JLab with 12 GeV has the ambition to go beyond these analyses. The PAC40 approved DVCS experiment in Hall C [7] is in the unique position, using the spectrometer capabilities in Hall C, to exploit the full kinematical dependence of the DVCS cross section in order to isolate all Fourier moments of the cross-section on an unpolarized target and separate the DVCS-BH interference and DVCS^2 contributions to each of them. Each individual term has a distinct Q^2 dependence that will be measured allowing one to quantify the size of higher-twist corrections. Notice that so far only the Q^2-dependence of the imaginary part of the DVCS amplitude has been studied experimentally [8]. The data showed indications of leading twist dominance. However, the test on several other observables including the real part of the DVCS amplitude, which is thus far not well understood, will be important for our global understanding of the GPD formalism. Precise study of Q^2 dependences and higher twists are of great interest for our global understanding. Twist-three GPDs can give access to a longitudinal proton spin sum rule [9] in a similar way as twist-2 GPDs probe the transverse spin through the well-know Ji sum rule [6]. The potential of DVCS to provide additional constraints on the real part of CFFs is important for developing more accurate GPD models and these data could also be used in global fits of CFFs and for dispersion relation analysis.

The energy separation requiring the measurements of conjugate settings (same Q^2 and x_B) at different beam energies is key to the overall DVCS program. With the CEBAF upgrade Hall C will receive electron beams of maximum energy of 11 GeV and luminosity of up to 10^{38} cm^{-2}

Table 1. Experiment requirements on $PbWO_4$.

Parameter	**Ideal**	**Acceptable**
Light Yield (pe/MeV)	10-15	5-6
Transmittance (20cm) at λ ∼420nm	>60%	∼40%
Uniformity of optical properties (%)	∼10	<20
Radiation hardness LY loss for 1.5 krad at dose rate 15 rad/h	5%	∼10%
Uniformity rad. degradation at the same dose (20%)	∼20	<30
Tolerance in dimensions (μm)	±50	±100
Timing property (ns, %)	30-50, 90%	

s^{-1} providing a great facility for the study of electron-nucleon scattering and for the separation of the DVCS cross section. Energy separation can only be performed with the high momentum spectrometers in Hall C due to the high momentum of scattered electrons increasing the Q^2 reach to even higher values at fixed x_B. Besides the requirement on momentum, efficient detection of photons is demanded over the entire kinematic range for the Hall C DVCS measurements to provide the highest precision data in the kinematic domain accessible with a 11 GeV beam extracting all possible independent observables on an unpolarized proton target.

The flexible design of the NPS allows other experiments to use its new capability of detecting neutral particles in Hall C as well. For instance, the PAC40 approved, A-rated SIDIS experiment [10], which probes the foundation of all SIDIS experiments at energies available at 12 GeV JLab, would be part of the same run group as DVCS and also use the NPS.

The neutral pion electroproduction SIDIS reaction plays a unique role in validating the SIDIS framework at JLab energies, and is thus an important tool in our study of hadron structure. The main advantages of neutral pion production include the lack of diffractive ρ contributions, the lack of pole contributions and thus radiative tail contributions at large z, the reduced nucleon resonance contribution (as for example compared to ep), and the proportionality to an average fragmentation function, are all points in favor to validate low-energy (x, z) factorization required to substantiate the SIDIS science output.

3. The Neutral Particle Spectrometer (NPS)

The basic concept for the NPS is a highly segmented electro-magnetic calorimeter preceded by a compact sweeping magnet. The experiments it enables, require detection of neutral particles with energies ranging between 0.5-7.6 GeV with good energy resolution (1-2%), and good coordinate (2-3 mm) and angular resolution of 0.5-0.75 mrad, which is comparable to the resolutions of the focusing spectrometers in Hall C. The neutral particle scattering angles cover 6.7-25 degrees at distances from the target ranging between 3 m and 6 m. For example, the minimum angle required at a distance of 4 m from the target is 7.2°.

The NPS is an efficient and economical way to meet all of the experimental requirements. It will consist of the following components:

- $PbWO_4$ crystals in a temperature controlled frame;
- a set of high voltage distribution bases with built-in amplifiers for operation in high-rate environments;
- essentially deadtime-less digitizing electronics to independently record the pulse amplitudes from each crystal;
- a sweeping magnet and a modified beam pipe with a large critical angle to minimize backgrounds that still reaches small angles and could be used as general purpose beam

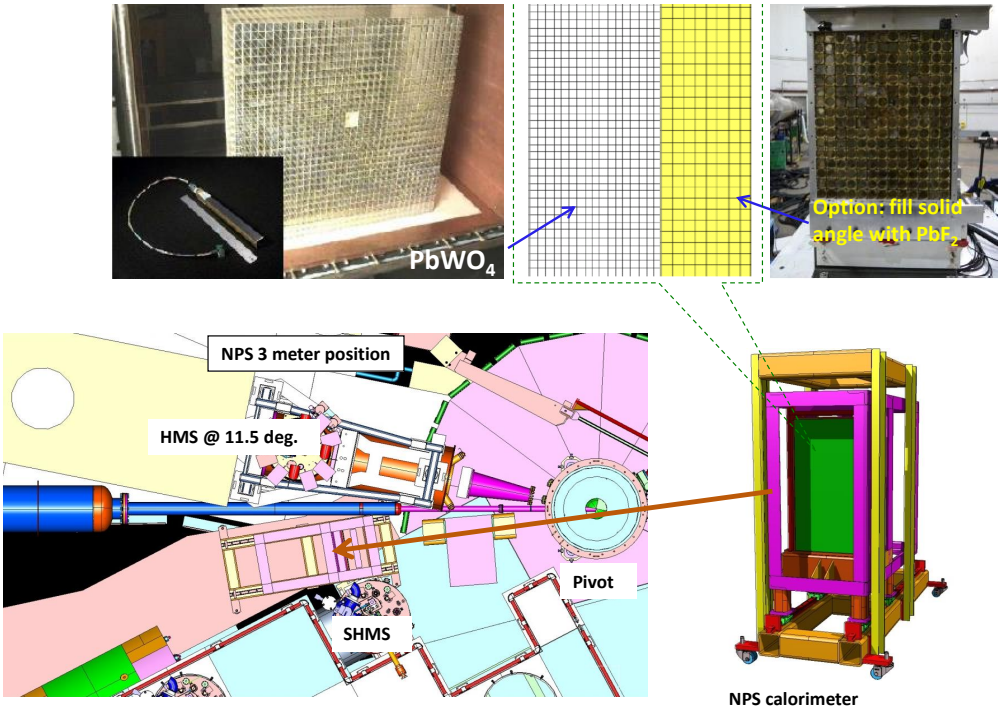

Figure 2. NPS crystal matrix and frame installation in Hall C.

pipe in Hall C ;

- a cantelevered platform of the SHMS carriage to allow precise, remote rotation around the Hall C pivot over an angular range between 6 and 25 degrees;
- a light monitoring and blue light curing system to monitor and restore crystal optical properties;

3.1. Crystals

The NPS will consist of an array of up to 1116 scintillating $PbWO_4$ and up to 208 PbF_2 crystals. Both types of crystals are fast ($PbWO_4$: 5-14 ns and PbF_2: $<$ 30ns) and so suitable for the experiments, which require fast signals with short tails to minimize pile-up at high rates, e.g., timing resolution of better than 100 ns [2]. The requirements of the NPS on PWO are summarized in Table 1. In general, the NPS needs crystals with high transparency, high light yield, good timing where 90% of the light is emitted within 30-50 ns, and good radiation hardness. Also important are crystal geometry and integrity.

In the ideal case the NPS calorimeter will consist of a set of brandnew $PbWO_4$ crystals. Taking advantage of the existing $PbWO_4$ crystals [3] of the high-resolution inner part of the Hybrid Electromagnetic Calorimeter (HYCAL) [12] used for PRIMEX /PRIMEX-II experiments one arrangement is an arrangement of 1080 scintillating $PbWO_4$ crystals in a 36 by 30 matrix covering 25 msr at a distance of 4 meters from the target. We could use the PbF_2 crystals from the Hall A DVCS calorimeter to fill out the solid angle if, in the worst case scenario, only around

[2] Bismuth Germanate (BGO), another commonly used scintillation crystal has a timing property of 300 ns and is thus not suitable for the NPS. LSO/LYSO is a crystal with acceptable timing, but is not an economically favorable option.

[3] and accompanying photomultiplier tubes (PMTs)

600 $PbWO_4$ crystals should be available due to scheduling conflicts. The remainder could then be replaced by 208 PbF_2 crystals in a hybrid configuration, one option of which arranging the faster $PbWO_4$ along the beam side is shown in Fig. 2 [4]. Such a hybrid spectrometer configuration with a combined crystal matrix was successfully used in the PrimEx HYCAL calorimeter, which had an inner core of $PbWO_4$ and an outer ring of lead glass crystals. Experience with the HYCAL yielded energy and coordinate resolutions of $\sigma/E = 1.3\%$ and σ_x ~1.28-2.10 mm at a neutral-pion energy of 5 GeV, giving an invariant mass distribution with a width of 2.3 MeV/c^2, which fully satisfies the needs of the DVCS and SIDIS π^0 experiments.

3.2. PMTs and amplifiers

The phototubes available with the $PbWO_4$ crystals from PrimEx, are the 10-stage Hamamatsu R4125 model with 19-mm diameter. For operation in the high-rate environment of the Hall C experiments, a new set of HV distribution bases with built-in amplifiers is needed. To increase the gain stability at the high rates anticipated with the NPS setup, the R4125 photomultiplier will be equipped with an active base [13]. The active base design improves gain stability with an efficient output signal range up to ~160 μA. In this range, the PMT base system gain, or pulse amplitude and pulse width, remains stable to within 1%. The measured pulse rate at this current corresponds to a rate of about 1.2 MHz of 300 mV output pulses. The total count rate advantage of the newly designed active base is a factor of ~25 as compared to the PrimEx base. It also indicates a noticeable improvement of the gain stability of the complete PMT plus base system versus count rate (or anode current). Additionally, radiation tests of the active PMT base were performed in Hall C during the Qweak operations in 2011/12 and no degradation of the base for a radiation dose of 100 kRad was found.

3.3. Trigger and electronics

The singles rate of electrons in the HMS for the experiment will be sufficiently low (<1kHz) to allow using a minimum-bias electron trigger and reading out the NPS in each event. In this way, exclusive, semi-inclusive, and inclusive cross sections can be compared directly at each kinematic point. To take full advantage of the high-resolution crystals while operating in a high-background environment, JLab-developed flash ADCs (fADCs) will be used to digitize the signal [5]. They continuously sample the signal every 4 ns, storing the information in an internal FPGA memory. When a trigger is received, the samples in a programmable window around the threshold crossing are read out for each crystal that fired. Since the readout of the FPGA does not interfere with the digitizations, the process is essentially deadtime free. If needed, the DAQ system will support windows up to 200-300 ns at 1 kHz and 100% occupancy in the 1200 channel calorimeter (~ 200 MB/s), but projected data rates will be smaller by orders of magnitude for all kinematics even if the thresholds are set very low. The sampled signals can then be fitted and integrated off-line, effectively eliminating issues with pile-ups, baseline shifts, etc. The fADC timing resolution was measured to be < 1 ns for all signals [22]. For low-Q^2 measurements, where the electron singles rate could be high, the fADC-based system can also support a coincidence trigger. Such a trigger would take advantage of the ability of the fADC to perform the integration of the pulse and pass it along to the trigger for cluster finding. The appropriate conditions for the latter can then be used to select, for instance, DVCS or π^0 events. The integration and cluster finding will delay the trigger decision, but this can be easily accommodated in a pipelined system without any need for delay cables or analog delay modules. In summary, the system will provide a low dead time, precision signal processing off-line, and support both high-rate operations in singles mode as well as advanced, trigger-level

[4] This option has the minimum number of transitions between the different block types

[5] The fADC250 modules [23] collect and process data with 10 or 12 bit resolution at 250 MHz sample rate.

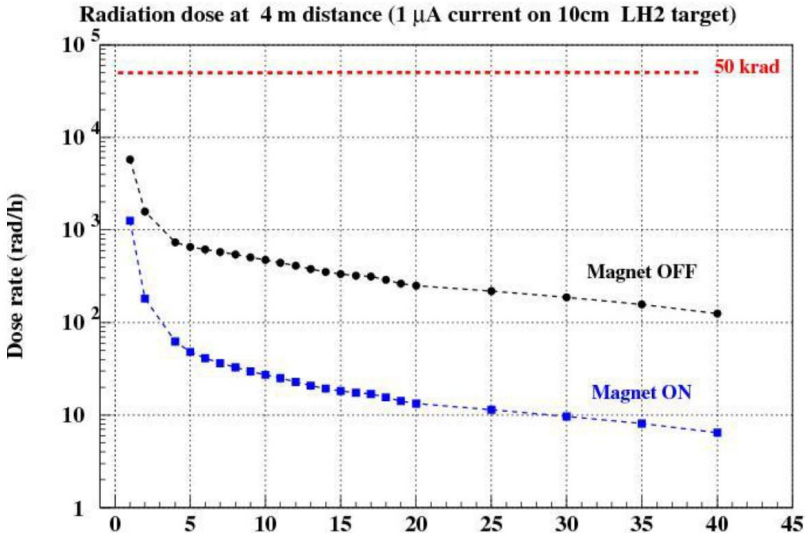

Figure 3. NPS crystal matrix and frame installation in Hall C.

cluster finding in coincidence mode.

3.4. Temperature controlled frame, cantilevered platform and positioning mechanism
The crystals will be installed in a frame based on that from the HyCal as shown in Figure 2. The detector frame will be mounted on a base frame with a rail system allowing the spectrometer to be moved in z to positions between 3 m and 12 m from the target.

The calorimeter box will be installed off a cantilevered platform on the SHMS (see Figure 2). It will rotate with the spectrometer allowing for precise positioning and eliminating the need for a separate motion control system, which is essential given the space constraints between the spectrometer and the beam line at small angles. In collaboration with the JLab engineering/design group we have analyzed the NPS positioning together with the other equipment in the experimental hall. The minimum central angles the NPS can reach fulfill all the requirements of DVCS experiment and SIDIS, and are also suitable for future experiments. The spectrometer will be designed so that it can be easily moved and removed from the SHMS platform.

The scintillation light output of the $PbWO_4$ crystals is temperature sensitive, and thus the entire calorimeter must be kept at a constant temperature (to within 0.1° to guarantee 0.5% energy stability for absolute calibration and resolution). Furthermore, the high-voltage dividers on the PMTs may dissipate a total of several hundred Watts, and this power must not create temperature gradients or instabilities in the calorimeter. The NPS will thus be thermally isolated and surrounded on all four sides by water cooled copper plates. This design is based on that of the HYCAL temperature controlled frame optimized with more recent experience from CMS [14], which has shown stability to 0.05°. The final choice of temperature will be a trade-off between light yield and radiation resistance. For $PbWO_4$ the light yield increases at lower temperatures, but luminescence decay time and radiation resistance decreases. The properties of PbF_2 are nearly independent of temperature.

4. Studies of backgrounds and radiation dose

To detect particles produced at small scattering angles, the Neutral Particle Spectrometer (NPS) must be installed close to the beamline. It is thus important to pay attention to the effect of

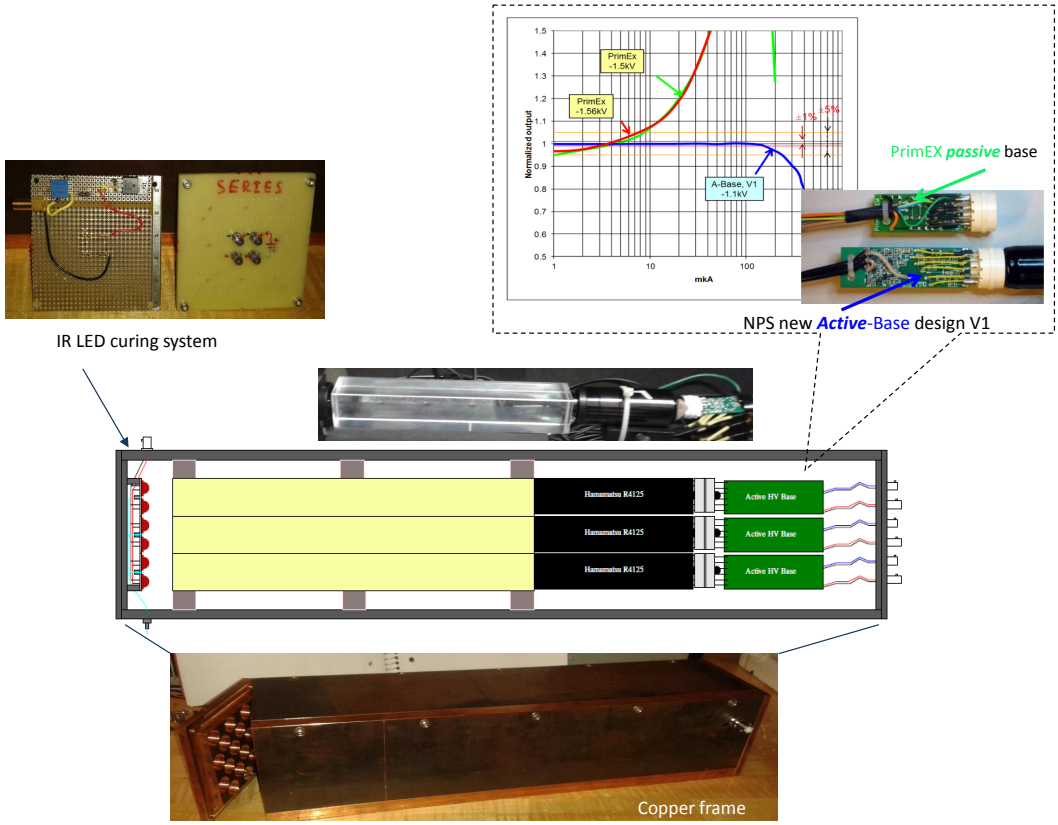

Figure 4. The NPS prototype. It consists of $PbWO_4$ and PbF_2 crystals in a copper frame. The readout is performed with R4125 with active bases. These active bases outperform the passive bases from PrimEx by about a factor of two. The setup also contains a prototype of the curing system.

radiation dose on the performance of the spectrometer. In particular, attention must be paid to degradation of the crystal optical properties and recovery thereof, and damage to the photosensors. The background rates could also directly affect the resolution of the spectrometer.

To select the optimal configuration for the NPS, simulations of the background rates and radiation doses were carried out. The baseline simulation is a well calibrated GEANT simulation used for all JLab offical dose rate estimates. It includes the 10 cm LH_2 target, a 0.3 T-m sweeping magnet, and the NPS, with its front face located at a distance of 4 meter from the target, covering an angular range between 5 and 25 degrees. The simulation showed a strong angular dependence of the background, and that the major fraction of the rate comes from Moeller electrons, which can be eliminated by the 0.3 Tm sweeping magnet. With the magnetic field added, the dominant parts of the beam-induced background rate become photons with an energy above 10 MeV and electrons with an energy above 100 MeV.

Radiation dose rates from the JLab official background simulation have been used to estimate the exact radiation condition as seen by the $PbWO_4$ detector as part of the NPS facility. Fig. 3 shows the total dose rates as a function of NPS angle, with magnet on and off, compared to a 50 krad dose limit before curing of the crystals is required. This number based on LHC studies [11] is conservative (i) even at much higher integrated doses only small (few %) effects are seen; (ii) additional shielding materials are not yet taken into account; and (iii) actual dose rates out-of-plane are much reduced. Additional and more detailed information on our background

and radiation dose studies can be found in Appendix VII of reference [10].

4.1. Light monitoring and curing system

The expected doses for the NPS experiments is dominated by small-angle operations, where the integrated dose is 1.7 Mrad in the center and 3.4 Mrad at the edge. To control the stability of the NPS and degradation of the crystals due to accumulated radiation dose a light monitoring system is needed. It will periodically inject light into detector modules between the real events during data taking or during special calibration runs with a frequency 10-20 Hz. Such a system will measure variations of the crystal transmittance over the course of the experiment and provide calibration in situ.

To restore the crystal optical properties, a curing system will be constructed with minimum impact on the experiment running. Our baseline method is to use blue light of wavelengths between 400-600 nm (optical bleaching [18]). The required light intensity is of an order of 1-2 mW/cm^2, and thus for the NPS 2x2 cm^2 ($PbWO_4$) or 3x3 cm^2 (PbF_2) crystals a curing system with power 5-10 mW/crystal (at wavelengths of 400-600 nm) is needed. This is a well established technique and has been used by many other experiments, e.g., GEP-III in Hall C and DVCS in Hall A. However, this technique is invasive and based on experience with the DVCS experiment can affect PMT operation. We will thus also develop a curing system with permanent infrared illumination based on those from, e.g., Refs. [20, 19, 21]. This method has been observed by the PANDA collaboration to yield significant improvement of the crystal optical transparency after being exposed to modest radiation doses.

5. NPS prototype studies

To optimize the technical aspects of the calorimeter before finalizing the NPS design a prototype has been constructed. As illustrated in Fig. 4 it has an active area of about 6x6 cm^2 including a crystal matrix of $PbWO_4$ (and PbF_2 to test the hybrid configuration) in a copper frame. The readout is done by 19 mm Hamamatsu R4125 PMTs with our new active HV base. The prototype will test the light monitoring system as well as two approaches for the curing system, i.e., standard with a blue light source and IR curing of wavelengths > 900 nm. The prototype IR curing system was constructed using superbright LEDs like the OSRAM LD274 with peak wavelength 950nm and Vishay TSAL7400 with peak wavelength 940nm.

The efficiency of IR curing is reduced by a factor 20-50 relative to blue light. This must be compensated by using high intensity ($\sim 10^{16}$ photons/s per crystal). We have measured the intensity of IR LEDs LD274 and TSAL7400 whose peak wavelenghts are around 950 nm. The measurements were done using a calibrated Hamamatsu silicone photodiode S2281 with quantum efficiency of 67% at 950nm to measure the intensity of the emitted light [6]. The distance betwen LED and photodiode was varied between 0.5 cm and 20 cm. The LED driving current was measured with a multimeter and the photodiode current was measured with a picoammeter. The results for the LED emission intensity as a function of driving current for distances from the photodiode of 3 cm and 7cm are shown in Fig. 5. The output is almost linear with driving current for both LEDs. Beyond 60 mA the output begins to curve slightly indicating the onset of saturation. Additional measurements with attenuation of the LEDs output light intensity were made with a neutral density filter with attenuation factor 9.25 installed in front of the LED. The data showed good agreement of the data without filter and with filter when scaled by the attenuation factor. The saturation does thus not seem to be due to the photodiode. The measured photon flux at LED driving current of 100 mA and 3 cm distance between the LED and the photodiode is equivalent to 2 x 10^{16} photons/s depositing a power of 4.2 mW/cm^2. The

[6] its current is nearly proportional to the LED intensity

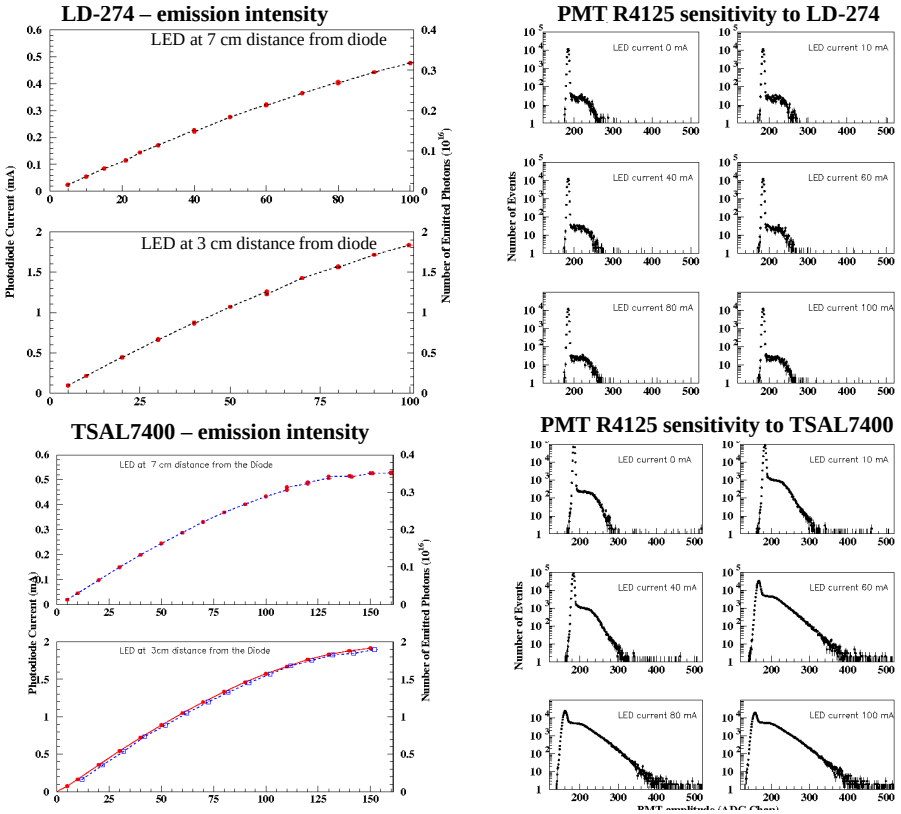

Figure 5. LEFT: the emission intensity of the IR LEDs LD274-3 (top figure) and TSAL7400 (bottom figure) vs. driving current at distances 7cm (top panels) and 3cm (bottom panels) and as indicated in the figure. The PMT HV for the measurements was 1600 V. The blue open symbols in the bottom figure denote data taken with a neutral density filter with attenuation factor 9.25 in front of the LED; RIGHT: the amplitude distributions of the signals detected by PMT R4125 at different values of the infrared LEDs driving currents (top: LD-274-3, bottom: TSAL7400).

photon flux at 7cm distance is 0.4 x 10^{16} photons/s. The results of the intensity tests suggest that both LEDs LD274 and TSAL7400 would be suitable for curing applications.

The possibility to perform continous curing of $PbWO_4$ using permanent illumination with infrared light when the PMT HV is on depends on the sensitivity of the PMTs to the IR light source. We have measured the PMT sensitivity to IR light. This is effectively a PMT quantum efficiency measurement at wavelength far beyond the sensitivity range shown in any of manufacturer data sheets. We have measured the PMT sensitivity at different driving LED currents between 0 and 100 mA for different configurations, e.g., distances between LED and PMT ranging between 0.5 cm and 18 cm, with and without the crystal in front of the PMT, and different PMT gains. The output signal was analyzed with an ADC of gate width 150 nsec, and 1 channel equivalent to 100 fC. The resulting signal amplitude distributions for different LED driving current (at different intensity of the IR light) are shown in Fig. 5. The data suggest that the PMT R4125 has a very low, but non-negligible efficiency to IR light. One thought about the PMT sensitivity is that the IR LED emission spectrum may be contamination by short wavelength light. Tests were thus repeated with a 900 nm long-pass filter cutting all wavelengths but IR. No difference between the measurements with and without filter were found.

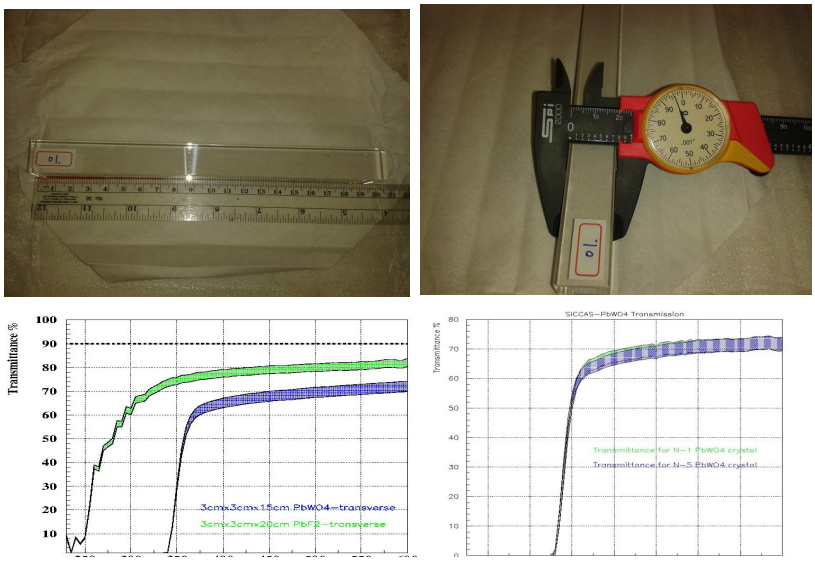

Figure 6. TOP LEFT/RIGHT: $PBWO_4$ crystal from SIC obtained in spring 2014. The measured dimensions are 20±0.15 mm x 20 ±0.15mm x 200mm. LEFT BOTTOM: The transmittance of PbF_2 from the Hall A DVCS calorimeter (green) and $PbWO_4$ from the HYCAL crystals vs. wavelength. The color band denotes the spread between the data measured at different points on the crystal. RIGHT BOTTOM: the transmittance for a $PbWO_4$ crystal from SIC obtained in spring 2014.

This suggests that the majority of the light has IR wavelengths, that the PMT has a real non-zero efficiency relative to IR light, and that the PMT could receive long term damage if left on during IR curing.

To estimate the effect of IR light on the PMT lifetime the relation between PMT anode current and LED driving current was analyzed. Measurements were made for 4 IR LEDs at 19cm distance from the PMT and an LED driving current of 50 mA. The PMT high voltages varied between 1400-1600 V, the typical operating voltages for these PMTs. For a 50mA LED driving current the 4-IR LEDs will have about $4x2x10^{16}$ photon/cm^2/s. The results are 309 nA for 1400 V, 492 nA for 1500 V and 758 nA for 1600 V. This is below the R4125 maximum anode current of $\sim$ 0.1 mA even for the highest voltages, and thus there will likely not be a large effect on the PMT lifetime. However, additional studies are ongoing to improve the PMT lifetime using LEDs with larger peak wavelengths, e.g., >1000 nm. The efficiency of curing with these IR LEDs will be tested with about 20krad irradiated crystals.

The $PbWO_4$ crystals used in the prototype were obtained from SIC in spring of 2014. The results of a transmittance measurement compared to the transmittance of crystals from the Hall C photon detector and PbF_2 crystals is shown in Fig. 6. The $PbWO_4$ and PbF_2 transmittance curves are very different in the short wavelength region (λ=250-350 nm), but for both types of crystals the transparency saturates for wavelengths above $\lambda \sim 400$ nm. A common blue light source should thus be acceptable for both types of crystals for the NPS light monitoring system. The efficiency of the blue light monitoring system will be tested with the prototype.

A prototype for electronics and triggering tests is being constructed to see how the fADC

based electronics would work with PbF_2. These pulses rise/fall faster than $PbWO_4$, which could result in fluctuations in the integral depending on the timing of the pulse with respect to the fADC clock. Furthermore, studies of existing elastic data from JLab are ongoing to check for possible impact on the resolution in timing and amplitude when doing a waveform analysis for PbF_2.

6. Acknowledgments

This work is supported in part by NSF grant PHY-1019521 and PHY-1036227, and Jefferson Science Associates (JSA).

7. Bibliography

[1] K. Goeke, M.V. Polyakov and M. Vanderhaeghen, Prog. Part. Nucl. Phys. **47**, 401 (2001)
[2] M. Diehl, Phys. Rept. **388**, 41 (2003).
[3] A.V. Belitsky and A.V. Radyushkin, Phys. Rept. **418**, 1 (2005).
[4] J.C. Collins, L. Frankfurt, M. Strikman, Phys. Rev. D **56**, 2982 (1997).
[5] J.C. Collins, A. Freund, Phys. Rev. D **59**, 074009 (1999).
[6] X. Ji, A. Freund, Phys. Rev. Lett. **78**, 610 (1997).
[7] A. Ahmidouch, I. Albayrak, D. Androic, J.R.M. Annand, A. Asaturyan, M. Ben Ali, M. Boer, A. Camsonne, M. Canan, M. Carmignotto, C. Chen, S. Covrig, S. Danagoulian, D. Day, M. Defurne, J. Denes-Couto, C. Desnault, R. Dupre, M. Elaasar, R. Ent, A. Fradi, M. Garcon, B. Garillon, D. Gaskell, L. Ghedira, F.X. Girod, P. Gueye, M. Guidal, D.J. Hamilton, Y. Han, M. Hattawy, N. Hlavin, T. Horn, G. Huber, C. Hyde, H.S. Jo, M. Jones, C. Keppel, P. King, D. Keller, F. Klein, P. E. C. Markowitz, A. Marti Jimenez-Arguello, M. Mazouz, A. Mkrtchyan, H. Mkrtchyan, C. Munoz-Camacho, P. Nadel-Turonski, B. Nepal, S. Niccolai, R. Paremuzyan, A.J.R. Puckett, M.N.H. Rashad, J. Roche, O. Rondon, F. Sabatie, B. Sawatzky, M.H. Shabestari, S. Sirca, P. Solvignon, V. Sulkosky, V. Tadevosyan, L. Tang, F. Wesselmann, S.A. Wood, B. Wojtsekhowski, S. Zhamkochyan, and the Neutral Particle Spectrometer Collaboration, *Approved Jefferson Lab experiment E12-13-010.*
http://www.jlab.org/exp_prog/proposals/13/PR12-13-010.pdf
[8] C. Muñoz Camacho, A. Camsonne, M. Mazouz, C. Ferdi, G. Gavalian, E. Kuchina, M. Amarian, K. A. Aniol, M. Beaumel, H. Benaoum, P. Bertin, M. Brossard, J.-P. Chen, E. Chudakov, B. Craver, F. Cusanno, C. W. de Jager, A. Deur, R. Feuerbach, J.-M. Fieschi, S. Frullani, M. Garçon, F. Garibaldi, O. Gayou, R. Gilman, J. Gomez, P. Gueye, P. A. M. Guichon, B. Guillon, O. Hansen, D. Hayes, D. Higinbotham, T. Holmstrom, C. E. Hyde-Wright, H. Ibrahim, R. Igarashi, X. Jiang, H. S. Jo, L. J. Kaufman, A. Kelleher, A. Kolarkar, G. Kumbartzki, G. Laveissière, J. J. LeRose, R. Lindgren, N. Liyanage, H.-J. Lu, D. J. Margaziotis, Z.-E. Meziani, K. McCormick, R. Michaels, B. Michel, B. Moffit, P. Monaghan, S. Nanda, V. Nelyubin, M. Potokar, Y. Qiang, R. D. Ransome, J.-S. Réal, B. Reitz, Y. Roblin, J. Roche, F. Sabatié, A. Saha, S. Sirca, K. Slifer, P. Solvignon, R. Subedi, V. Sulkosky, P. E. Ulmer, E. Voutier, K. Wang, L. B. Weinstein, B. Wojtsekhowski, X. Zheng, and L. Zhu [Jefferson Lab Hall A Collaboration], Phys. Rev. Lett. **97**, 262002 (2006)
[9] X. Ji, X. Xiong, F. Yuan, Phys. Rev. Lett. **109**, 152005 (2012).
[10] A. Ahmidouch, I. Albayrak, D. Androic, A. Asaturyan, F. Benmokthar, A. Camsonne, M. Carmignotto, C. Chen, M. E. Christy, S. Covrig, S. Danagoulian, D. Day, P. Degtiarenko, J. Denes-Couto, D. Dutta, J. Dunne, M. Elaasar, R. Ent, D. Gaskell, D.J. Hamilton, Y. Han, D.W. Higinbotham, M. Guidal, N. Hlavin, T. Horn, G. Huber, C. Hyde, M. Jones, N. Kalantarians, D. Keller, C. Keppel, M. Khachatryan, P. King, F. Klein, M. Kohl, V. Kubarovsky, W. Li, P. E. C. Markowitz, M. Metz, A. Mkrtchyan, H. Mkrtchyan, C. Munoz-Camacho, P. Nadel-Turonski, B. Nepal, R. Paremuzyan, M.N.H. Rashad, J. Roche, O. Rondon, B. Sawatzky, M.H. Shabestari, S. Sirca, P. Solvignon, V. Tadevosyan, L. Tang, J. Taylor, F. Wesselmann, S.A. Wood, B. Wojtsekhowski, S. Zhamkochyan, and the Neutral Particle Spectrometer Collaboration, *Approved Jefferson Lab experiment E12-13-007.*
http://www.jlab.org/exp_prog/proposals/13/PR12-13-007.pdf
http://www.jlab.org/exp_prog/proposals/09/PR12-09-011.pdf
[11] R.Y. Zhu et al., *Nucl. Inst.Meth* A**413**, 297 (1998).
[12] M. Kubantsev et al., Performance of the Primex Electromagnetic Calorimeter, arXiv:physics/0609201, 22 Sep. 2006; A. Gasparyan, Performance of PWO crystal Detector for a High Resolution Hybrit Electromagnetic Calorimeter at Jefferson Lab., Proceed. X Int. Conf. Calorimetry in Particle Physics, Perugia, Italy, 29 March-2 April 2004, pp. 109-115.

[13] V. Popov and H. Mkrtchyan, New potomultiplier active base for Hall C Jefferson Lab Lead Tangstate Calorimeter, NSSS2012-1098.
[14] G. Franzoni et.al, *Nucl. Instrum. Meth.* A **628**, 90 (2011).
[15] V. A. Batarin et.al, (BTeV electromagnetic calorimeter group), Nucl. Instrum. Meth. A512, 488 (2003), hep-ex/0210011.
[16] P. Adzic et.al, The CMS Electromagnetic Calorimeter Group Report, http:iopscience.iop.org1748-0221503P0310, 2010.
[17] Qu Xiangdong, A Study of Lead Tungstate Crystals and Improvement of Radiation Hardness. Ph.D. Thesis, Shanghai Institute of Ceramics. The Chinese Academy of Sciences, Shanghai, China, January 16, 2001.
[18] R.Y. Zhu et al., *Nucl. Instrum. and Meth.* A **376**, 319 (1996); C. Woody et al., Proc. of SCINT95 Int'l Conf. Delft, August 1995 and IEEE-NUCL-S V 43 (1996) 1585.
[19] M. Anfreville et al., Nucl. Inst.Meth A**594**, 292 (2008).
[20] R.W. Novotny, PANDA collaboration, IEEE-2009-05402124.
[21] D.A. Mao et al., Nucl. Inst.Meth A**356**, 309 (1995).
[22] J.V. Bennett, M. Kornicer, M.R. Shepherd, M.M. Ito, "Precision timing measurements of phototube pulses using a flash analog-to-digital converter", JLab technical report (2013).
[23] H. Dong, C. Cuevas, D. Curry, E. Jastrzembski, F. Barbosa, J. Wilson, M. Taylor, and B. Raydo, IEEE Nuclear Science Symposium Conference Record, N15-375 (2007).